Analysis of Eddy-Current Losses Over Conductive Substrates with Applications to Monolithic Inductors and Transformers

Ali M. Niknejad, *Member, IEEE,* and Robert G. Meyer, *Fellow, IEEE*

***Abstract*—In this paper, a closed-form integral representation for the eddy-current losses over a conductive substrate is presented. The results are applicable to monolithic inductors and transformers, especially when such structures are realized over an epitaxial CMOS substrate. The technique is verified against measured results from 100 MHz to 14 GHz for spiral inductors.**

***Index Terms*—CMOS substrate losses, eddy currents, monolithic inductors, monolithic transformers, spiral inductors, spiral transformers.**

I. Introduction

MONOLITHIC inductors and transformers, especially in the form of spirals, have gained great importance in the design of integrated silicon RF transmitters and receivers. For this reason, the analysis and optimization of such structures has been of paramount importance.

The optimization of these structures involves maximizing the quality factor Q of these devices, or equivalently, maximizing the magnetic or electromagnetic energy stored by the structures while minimizing the energy dissipation. There are several mechanisms for energy dissipation. At the frequencies of interest, in the dc–15-GHz range, the most important losses occur in the metal layers that form the devices, as well as in the bulk Si substrate that appears below the device.

Due to the nonzero resistivity of the metal layers, there are ohmic losses in the metal traces as well as eddy-current losses. The eddy currents in the metal traces arise from the magnetic field generated by the device that penetrates the metal layers. These magnetic fields induce currents that give rise to a nonuniform current distribution along the width and thickness of conductors, pushing current to the outer skin of the conductors. These effects are also known as skin and proximity effects. Skin-effect losses are from the magnetic field of the "self"-inductance of a metal trace, whereas proximity effects result from the magnetic field of nearby conductors. The proximity of nearby conductors also contributes to the current distribution in a conductor, most prominently for the innermost turns of spiral where the magnetic field is strongest [1], [2]. This leads to more pronounced current constriction along the inner core of the spiral.

In a previous paper [3], a technique was presented to analyze the skin- and proximity-effect losses based on the previous work of [4] and [5], especially the partial-element equivalent-circuit (PEEC) formulation [6]. Electrical substrate losses were also analyzed in [3] based on the work of [7] and [8]. Eddy-current losses in the bulk Si substrate, though, were not accounted for, as a free-space Green function was used to derive the inductance. In this paper, previous work is extended by including the magnetically induced losses in the substrate.

The importance of modeling such effects was not initially realized, as these effects were not widely observable in the bipolar and BiCMOS substrates of interest because of the widespread use of highly resistive bulk materials. These effects, though, were seen to be of integral importance when researchers attempted the construction of high-Q inductors over an epitaxial CMOS substrate [9]. In [1], the importance of modeling eddy currents was further demonstrated through numerical electromagnetic simulation. These simulations and measurement results clearly show that eddy currents are a dominant source of loss in these substrates.

In this paper, approximate two-dimensional (2-D) expressions for the eddy-current losses over a multilayer substrate are derived. These can be used to predict the losses in inductors and transformers fabricated over such substrates. In Section II, the results are derived using quasi-static analysis. In Section III, the losses at low frequency are calculated, and in Section IV, the results are extended to high frequency. Finally, in Section V, the results are compared to measurement.

II. Electromagnetic Formulation

A. Partial Differential Equations for Scalar and Vector Potential

Consider a long filament sitting on top of a multilayer substrate. A cross section of the geometry is shown in Fig. 1. Assume the filament is carrying a time–harmonic current. The substrate is assumed infinite in extent in the traverse direction, whereas each substrate layer k has thickness t_k, conductivity σ_k, magnetic permeability μ_k, and electric permittivity ϵ_k. The substrate is most likely nonmagnetic or weakly diamagnetic, a good approximation for Si and other semiconductors. The introduction of a linear magnetic substrate, though, does not complicate the analysis. The filament is located a distance b above the substrate, parallel to the z-direction.

Manuscript received October 6, 1999. This work was supported by the Defense Advanced Research Projects Agency under Project F30602-97-2-0346.

A. M. Niknejad was with the Berkeley Wireless Research Center, University of California at Berkeley, Berkeley, CA 94720 USA. He is now with Silicon Laboratories, Austin, TX 78735 USA (e-mail: amn@silabs.com).

R. G. Meyer is with the Berkeley Wireless Research Center, University of California at Berkeley, Berkeley, CA 94720 USA (e-mail: rmeyer@eecs.berkeley.edu).

Publisher Item Identifier S 0018-9480(01)00019-9.

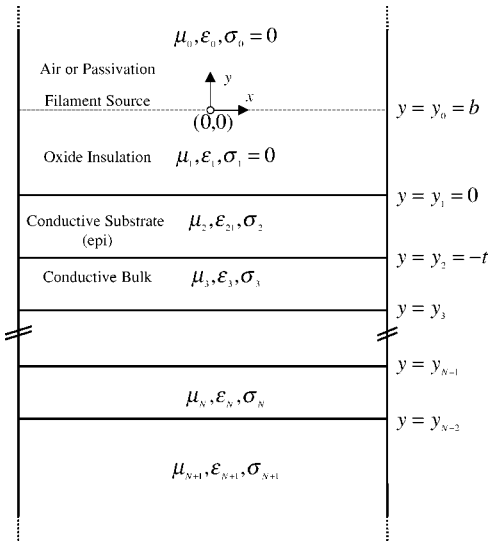

Fig. 1. Multilayer substrate excited by a filamental current source.

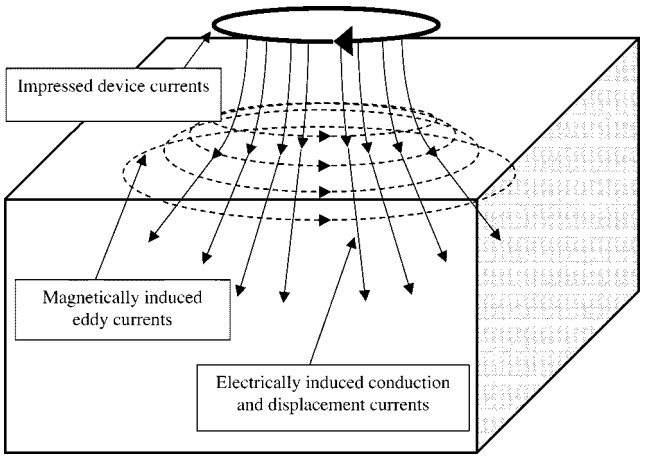

Fig. 2. Schematic representation of electrically and magnetically induced currents.

The electric and magnetic fields are completely determined by Maxwell's equation. The time–harmonic fields are determined by the scalar and vector potentials [10]

$$E = -j\omega A - \nabla\phi \tag{1}$$

$$B = \nabla \times A. \tag{2}$$

For obvious reasons, we will denote the first term of (1) the magnetic response and the second term of (1) the electric response. From Maxwell's equations, we have the well-known relation

$$\nabla(\nabla \cdot A) - \nabla^2 A = \mu J + j\omega\mu\epsilon E. \tag{3}$$

Assuming the substrate and metal conductors are linear and isotropic gives

$$J = \sigma E + J_{src}. \tag{4}$$

Substituting (4) and (1) in (3) and invoking a coulomb gauge results in the following:

$$\nabla^2 A = \mu(j\omega\sigma A - \omega^2\epsilon A(\sigma + j\omega\epsilon)\nabla\phi - J_{src}). \tag{5}$$

The parenthetical expression on the right-hand side has units of current density. The first term can be identified as the magnetically induced eddy currents that flow in the substrate and metal conductors. The second term is the dynamic radiation current term. The third term includes the electrically induced conductive and displacement currents flowing in the substrate. Finally, the last term is the impressed currents flowing in the metal conductors.

At microwave frequencies of interest (<15 GHz), the constant of the second term is at least three orders of magnitude smaller than the first, and can be safely ignored. The physical significance is that radiation is negligible. Dropping the third term of (5) has two implications. First, the magnetic-field contribution of the electrically induced currents will be ignored. Second, the electrically induced substrate losses will be ignored. The second implication is a far bigger concern as the electrically induced substrate losses are significant at frequencies of interest. The contribution to the magnetic field, though, can be safely ignored. To understand this physically, consider the schematic representation of the substrate currents shown in Fig. 2. Clearly, the electrically induced current distribution leads to a zero magnetic field. This can be shown at low frequency by noting that $\nabla \times \nabla\phi \equiv 0$.

Applying the coulomb gauge to the electric divergence relation, we obtain the well-known electrostatic Poisson's equation

$$\nabla \cdot E = \nabla \cdot (-j\omega A - \nabla\phi) = -\nabla^2\phi = \rho/\epsilon. \tag{6}$$

If we modify the above equation by replacing the electric permittivity with

$$\epsilon = \epsilon' + j\epsilon'' - j\frac{\sigma}{\omega} \tag{7}$$

we account for the loss tangent of the material as well as the conductive losses. Thus, the electrically induced losses can be derived from (6) instead of (5). This is valid as long as skin effect in the bulk does not significantly alter the electrically induced current distribution in the substrate. With these simplifications, we have

$$\nabla^2\phi = \frac{\rho}{\epsilon} \tag{8}$$

$$(\nabla^2 - \gamma^2)A = \mu J_{src} \tag{9}$$

where

$$\gamma^2 = \mu\epsilon\omega^2 - j\omega\sigma \tag{10}$$

and ϵ is given by (7).

B. Boundary Value Problem for Single Filament

Under a 2-D approximation, the magnetic vector potential is directed in the direction of current and, hence, has only a nonzero component in the z-direction. At microwave frequencies of interest, (9) simplifies and for each region

$$\nabla^2 A_k = j\omega\mu_k\sigma_k A_k. \tag{11}$$

By the method of separation of variables in rectangular coordinates [11], we write the solution in each layer as follows:

$$A_k(x, y) = X_k(x)Y_k(y)\hat{z}. \tag{12}$$

Substitution of the above form in (11) produces two ordinary constant-coefficient second-order differential equations

$$\frac{d^2X_k}{dx^2} = -m^2 X_k \tag{13}$$

$$\frac{d^2Y_k}{dy^2} = -\gamma_k^2 Y_k \tag{14}$$

with the additional constraint that

$$\gamma_k^2 - m^2 = j\omega\mu_k\sigma_k. \tag{15}$$

Due to the even symmetry of the problem, one selects

$$X_k = \cos(mx) \tag{16}$$

and by (15), it follows that

$$Y_k = M_k e^{\gamma_k y} + N_k e^{-\gamma_k y}. \tag{17}$$

Since we seek the vector potential over an infinite domain, the most general solution has the following form:

$$A_k(x, y) = \int_0^\infty (M_k e^{\gamma_k y} + N_k e^{-\gamma_k y}) \cos mx\, dm. \tag{18}$$

For N conductive layers, there are $2(N+2)$ unknown coefficients in the expansion of (18). There are $2(N+1)$ boundary conditions, which hold at the interface of each layers. The boundary conditions follow from Maxwell's equations [10]

$$(B_{k+1} - B_k) \cdot \hat{n} = 0 \tag{19}$$

$$(H_{k+1} - H_k) \times \hat{n} = K \tag{20}$$

where K is the surface current density. For $k \geq 1$, the above relations simplify to

$$B_{k,y} = B_{k+1,y} \tag{21}$$

$$\frac{1}{\mu_k} B_{k,x} = \frac{1}{\mu_{k+1}} B_{k+1,x} \tag{22}$$

where

$$B_k = \nabla \times (A_k \hat{z}) \tag{23}$$

$$H_k = \frac{1}{\mu_k} B_k. \tag{24}$$

Note that (21) and (22) must hold for each mode of (18) so one can show that

$$\begin{pmatrix} M_{k+1} \\ N_{k+1} \end{pmatrix} = \frac{1}{2} \begin{pmatrix} (1+\lambda_k)e^{-g_k} & (1-\lambda_k)e^{-h_k} \\ (1-\lambda_k)e^{+h_k} & (1+\lambda_k)e^{+g_k} \end{pmatrix} \begin{pmatrix} M_k \\ N_k \end{pmatrix} \tag{25}$$

where

$$\lambda_k = \frac{\mu_{k+1}}{\mu_k} \frac{\gamma_k}{\gamma_{k+1}} \tag{26}$$

and

$$g_k = (\gamma_{k+1} - \gamma_k) y_k \tag{27}$$

$$h_k = (\gamma_{k+1} + \gamma_k) y_k. \tag{28}$$

Since $A \to 0$ as $y \to \pm\infty$, it follows that $M_0 \equiv 0$ and $N_{N+1} \equiv 0$ to satisfy the boundary condition at infinity.

The boundary conditions at the filament interface $y = b$ require special care. Applying (21) and (22), we have [12]

$$\frac{1}{\mu_0} \frac{\partial A_0}{\partial x}\bigg|_{y=b} = \frac{1}{\mu_1} \frac{\partial A_1}{\partial x}\bigg|_{y=b} \tag{29}$$

$$\left(\frac{1}{\mu_0} \frac{\partial A_0}{\partial y} - \frac{1}{\mu_1} \frac{\partial A_1}{\partial y} \right]_{y=b} = K(x) \tag{30}$$

where

$$K(x) = \delta(x) I \tag{31}$$

or, equivalently, expressing (31) as an inverse cosine transform

$$K(x) = \frac{I}{\pi} \int_0^\infty \cos mx\, dm. \tag{32}$$

Thus, all the unknown coefficients may be evaluated and the boundary value problem is solved. This is the approach followed in [12] and [13]. An alternative derivation, which leads to a different integral representation of the magnetic potential, is presented in [14]. Observe that the magnetic field in the free-space region above the substrate may be expressed as arising from two sources: the filament current and the currents flowing in the substrate (the eddy currents). To derive the term arising from the filament in free space, observe that

$$B(r) = \frac{\mu_0 I}{2\pi r} \tag{33}$$

which may be expressed by the converging Fourier integrals

$$B_{0x} = \frac{\mu_0 I}{2\pi} \int e^{-|b-y|m} \cos mx\, dm \tag{34}$$

$$B_{0xy} = \frac{\mu_0 I}{2\pi} \int e^{-|b-y|m} \sin mx\, dm. \tag{35}$$

This observation implies that

$$M_0(m) = \frac{\mu_0 I}{2\pi} \frac{e^{-bm}}{m}. \tag{36}$$

Using the above relation and (29), the coefficients can be obtained uniquely for all layers. More generally, we can write

$$A(x, y) = \frac{\mu I}{2\pi} \int_0^\infty \frac{e^{m|y-y_0|}}{m} \big(1 + \Gamma(m)\big) \cos\big(m(x - x_0)\big)\, dm \tag{37}$$

where (x_0, y_0) is the source filament location. The unity term accounts for the filament current in free space and the term involving Γ accounts for the eddy currents in the substrate. In other words, the first term is the solution of the free-space problem for the impressed filamental currents, whereas the second term is due to the response eddy currents in the substrate. This particular form will be very fruitful in the analysis that follows.

C. Problems Involving Circular Symmetry

When the current excitation is circular or approximately symmetric, as in the case of a polygon spiral inductor, the assumption of circular symmetry also leads to a one-dimensional integral expression for the magnetic vector potential. The analogous solution involves Bessel functions in the place of the co-

sine function of (37). This problem has been treated extensively in [14]–[16] using a magnetostatic formulation, and in [17] and [18] using an electromagnetic formulation. In this paper, we will concentrate on the infinite rectangular solution as it applies more directly to devices involving orthogonal or Manhattan geometry. It should also be noted that [19] used the circularly symmetric solution to calculate the substrate losses.

III. Eddy-Current Losses at Low Frequency

A. Eddy-Current Losses for Filaments

With the magnetic vector potential known, we can proceed to calculate the eddy-current losses. There are two approaches to determine the losses. One approach is to use Poynting's theorem to calculate the total power crossing a surface enclosing the filament. In the time–harmonic case, the real component of this power must be due to the lossy substrate since no other loss mechanisms are present [14]. The complex Poynting's vector is given by

$$S = \frac{1}{2}(E \times H^*). \tag{38}$$

If we integrate the normal component of this vector over the surface $y = 0$, we obtain the power crossing the substrate

$$P + jQ = \frac{1}{2} \int_{-\infty}^{\infty} (E \times H^*) \cdot \hat{y}\, dx. \tag{39}$$

Considering now only the magnetic response of the substrate, from (1), we have

$$E = -j\omega A. \tag{40}$$

Thus, (38) becomes

$$S = \frac{-j\omega}{2\mu} A \times \nabla \times A. \tag{41}$$

For the geometry of Fig. 1, the integrand of (39) simplifies to

$$(E \times H^*) \cdot \hat{y} = \frac{-j\omega}{\mu} A \frac{\partial A^*}{\partial y}. \tag{42}$$

In Section II-B, it was shown that the magnetic vector potential has the following general form:

$$A(x, y) = \frac{\mu I}{2\pi} \int_0^{\infty} f(y, m) \cos mx\, dm. \tag{43}$$

Differentiating (43) under the integral and substituting in (39) results in

$$P + jQ = \frac{-j\omega}{2\mu} \int_{-\infty}^{\infty} dx \left[\frac{\mu I}{2\pi} \int_0^{\infty} \frac{\partial f(y, n)^*}{\partial y} \cos nx\, dn \right] \times \left[\frac{\mu I}{2\pi} \int_0^{\infty} f(y, m) \cos mx\, dm \right]. \tag{44}$$

If we interchange the order of integration and observe that

$$\begin{aligned} &\lim_{L\to\infty} \int_{-L}^{L} \cos mx \cos nx\, dx \\ &\quad = \lim_{L\to\infty} \left[\frac{\sin L(m-n)}{m-n} + \frac{\sin L(m+n)}{m+n} \right] \\ &\quad = \pi\big(\delta(m-n) + \delta(m+n)\big) \end{aligned} \tag{45}$$

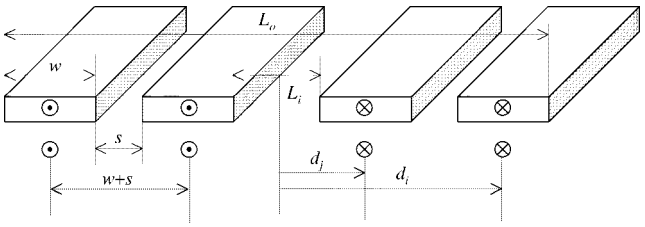

Fig. 3. Cross section of square spiral inductor.

we obtain

$$P + jQ = \frac{-j\omega\mu I^2}{8\pi} \int_0^{\infty} f(y, m) f_y^*(y, m)\, dm. \tag{46}$$

Thus, the equivalent resistance per unit length seen by the source driving the filament becomes

$$R_{\text{eq}} = \Re\big[2(P + jQ)\big]/I^2. \tag{47}$$

The imaginary part of (47) also contains useful information as it represents the reactive power crossing the surface that can be attributed to inductance. This is a negative increasing function of frequency that represents decreasing inductance as a function of frequency. The inductance decreases due to the "image" eddy currents flowing in the substrate. By Lenz's law, these currents flow in a direction opposite to the impressed current and, hence, generate a magnetic field that tends to cancel the penetrating magnetic field of the source, thereby decreasing the inductance.

Using this principle, let us derive the power loss for the configuration shown in Fig. 3. Note that two sets of N parallel current filaments carry a current I where the individual filaments are separated by a distance s and the two sets of filaments are separated by a distance d. Notice that this current distribution crudely approximates one-half of the current distribution for a spiral inductor of N turns. In a spiral inductor, the filaments have finite length and vary in length. Here, we neglect "end effects" and calculate the losses for the average length filament.

Using (43), we have

$$A(x, y) = \frac{\mu_0 I}{2\pi} \int_0^{\infty} f(y, m) \times \left(\sum_{i=1}^{N} \cos m(x - d_i) - \cos m(x + d_i) \right) dm \tag{48}$$

and

$$A_y^*(x, y) = \frac{\mu_0 I}{2\pi} \int_0^{\infty} f_y^*(y, n) \times \left(\sum_{i=1}^{N} \cos n(x - d_i) - \cos n(x + d_i) \right) dn \tag{49}$$

and applying (46) while changing the order of integration, we have

$$P + jQ = \frac{\mu_0^2 I^2}{4\pi^2} \int_0^{\infty} \int_0^{\infty} f_y^*(m) f(n) \cdot \left(\int_{-\infty}^{\infty} H(x)\, dx \right) dm\, dn \tag{50}$$

where

$$H(x) = \sum_{i,j} \pm \cos\big(n(x \pm d_i)\big) \cos\big(m(x \pm d_j)\big) \tag{51}$$

has been written in shorthand notation. Each x domain integral of (50) takes the form of

$$\int_{-\infty}^{\infty} \cos m(x+\alpha) \cos n(x+\beta)\, dx = \delta(m-n)\cos(m\alpha+n\beta)\pi + \delta(m+n)\cos(m\alpha-n\beta)\pi. \tag{52}$$

Using the above relation reduces (50) to

$$P + jQ = \frac{\mu_0^2 I^2}{\pi} \int_0^{\infty} f_y^*(m) f(n) \times \left(\sum_{i,j} \sin(m d_j) \sin(m d_i) \right) dm\, dn. \tag{53}$$

Alternatively, one can derive the equivalent impedance per unit length seen by the source driving the filament by simply observing that, by (1), the reflected magnetic contribution to the impedance must be [12]

$$R_{\text{eq}} = \Re\left[\frac{j\omega A_0(0, b)}{I} \right]. \tag{54}$$

Notice that (54) will lead to a different, yet equivalent, integral expression for the eddy-current losses.

B. Eddy-Current Losses for Conductors

Due to the linearity of Maxwell's equations, we can invoke the superposition principle to calculate the losses when more than one filament is present, even for a continuous distribution of the field. An alternative viewpoint is that, in calculating the vector potential for the filament case, we have actually derived the kernel of the integral operator that is the inverse transform of (11) or the 2-D Green function [20].

Thus, for any 2-D distribution of current over the multilayer substrate of Fig. 1, we can write the resulting vector potential as[1]

$$A(x, y) = \iint G(x, y) J(x, y)\, dS \tag{55}$$

where the surface integral is taken over the cross section of the conductor and has the form of (43). If the current distribution is uniform, this simplifies to

$$A(x, y) = I \iint G(x, y)\, dS. \tag{56}$$

In many practical cases, the current distribution is nonuniform. In these cases, one may approximate the current distribution by dividing the cross section into uniform current distribution segments and apply (56) to such segments. This is discussed in more detail in [3], [5], [6], and [21]. Integrating (43) over the width w of the source conductor, we obtain

$$A_w(x, y) = \frac{\mu I}{2\pi} \int_0^{\infty} f(y, m) \left[\frac{\sin \frac{mw}{2}}{\frac{mw}{2}} \right] \cos mx\, dm. \tag{57}$$

If we further average the above expression over the finite width of the field point, we obtain

$$A_{ww}(x, y) = \frac{\mu I}{2\pi} \int_0^{\infty} f(y, m) \left[\frac{\sin \frac{mw}{2}}{\frac{mw}{2}} \right]^2 \cos mx\, dm \tag{58}$$

assuming the field conductor width is also equal to w.

In order to calculate the total impedance for a set of filaments in series, one must account for the self- and mutual-impedance terms

$$Z_{\text{eq}} = \sum_{i,j} \frac{j\omega A_j(d_i, b)}{I} = \sum_{i,j} Z_{ij} \eta_j \tag{59}$$

where $A_j(d_i, b)$ is the vector potential generated by the jth conductor evaluated at the location of conductor i and is given by

$$A_j^{\pm}(d_i, b) = \pm \frac{\mu I}{2\pi} \int_0^{\infty} f(b, m) \cos m(d_i - d_j)\, dm \tag{60}$$

where the positive sign is used when the currents flow in the same direction, whereas the negative sign is used when the currents flow in opposite directions.

The factor $\eta_i = I_i/I$ accounts for the nonuniform current distribution along the length of the device. At low frequencies, $\eta_i \approx 1\ \forall\ i$ since no current is lost to the substrate due to displacement current. At higher frequencies, though, it is critical to evaluate (59) with this factor in place as the current distribution becomes nonuniform. In Section IV, we derive this current distribution.

IV. Eddy Currents at High Frequency

A. Assumptions

In [6], the PEEC formulation is shown to be equivalent to solving Maxwell's equation. We can thus formulate our problem using a modified PEEC technique. Our modifications mainly take advantage of the special geometry and symmetries in the problem to reduce the calculations. This approach has already been pursued in [3]. Here, we present a more symmetric formulation.

First, we would like to avoid generating volume elements in the substrate. Generating volume elements in the substrate would allow free-space Green functions to be employed, but this would produce too many elements. Since the Si substrate is only moderately conductive, we would require several skin depths of thickness in the substrate volume, as well as an area at least two to three times the area of the device under investigation to include the fringing fields. Since the fields vary rapidly across the cross-sectional area and depth of the substrate, many mesh points would be required. On the other hand, if we formulate the problem with a multilayer Green function, the substrate

[1]Note that this is not, in general, true for the vector potential since a dyadic Green function must be employed. However, it is valid for the 2-D case under investigation.

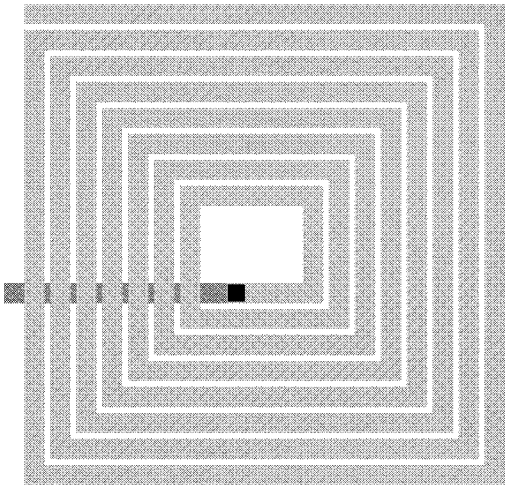

Fig. 4. Layout of $L27$ inductor.

effects are taken care of automatically and the substrate can be effectively ignored in the calculation. Therefore, only the conductor volumes need to be meshed.

Furthermore, since the conductors that make up the device are good conductors, consisting primarily of aluminum, gold, or copper, displacement current in the volume of the conductors can be safely ignored. Thus, the divergenceless current distribution in the conductors is found solely by solving the magnetostatic problem (9). The divergence of the current is determined from the electrostatic distribution of charge found by solving (8).

One further assumption greatly reduces the order of the problem. If we assume that the current flows along the length of the conductors in a one-dimensional fashion, then only meshing in one dimension as opposed to two or three dimensions is needed. For a typical spiral shown in Fig. 4, we see that this is indeed a good approximation. Note that this does not preclude a nonuniform current distribution along the length, width, or thickness of the conductors. Rather, the current is constrained to flow in one direction only. This assumption is mostly in error around the corners of the device where we may choose to use a 2-D current distribution or we may simply ignore the corner contributions.

B. Partial Inductance Matrix

Given the assumptions of Section IV-A, we may subdivide the device into many sub-conductors, as shown in Fig. 5. Since the current is constrained to flow in one dimension, the problem can be reduced by solving the equivalent magnetic circuit equations. For the system of filaments, we calculate a partial inductance matrix $\tilde{Z}^M$ [4] where each nondiagonal element is computed with

$$\tilde{Z}^M_{i,j} = j\omega \int_{C_i} A_j \cdot dl_i \tag{61}$$

and the diagonal elements are given by

$$\tilde{Z}^M_{i,j} = R_i + j\omega \int_{C_i} A_i \cdot dl_i. \tag{62}$$

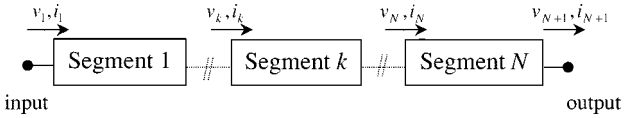

Fig. 5. Voltages and currents along series-connected two-port elements.

Employing the same approximations as [5], we reduce this matrix to the level of the conductors by invoking Kirchhoff's current law (KCL), at each node, to obtain [21]

$$Z^M = \left(S^T \left(\tilde{Z}^M\right)^{-1} S\right)^{-1} \tag{63}$$

where the sparse rectangular matrix S sums over the current sub-elements of a conductor. Thus, each row has a one in a position corresponding to a sub-element and zero otherwise. The problem with computing (63) directly is that the large matrix $\tilde{Z}^M$ must be computed and inverted.

C. Fast Computation of the Partial Inductance Matrix

In [21], computation of (63) is avoided altogether by an iterative solution. The matrix–vector products are accelerated by taking advantage of the $1/r$ form of the free-space kernel [22]. This kernel specialization, though, limits the applicability of the technique and precludes its application to the problem at hand since this would require us to either ignore the Si substrate (which distorts the free-space Green's function) or to mesh the substrate. Not only does the substrate meshing unnecessarily increase the size of the problem, but it also requires a more complete PEEC formulation since displacement current cannot be ignored in the substrate.

The authors of [23] have developed a more general iterative solver that can be applied to (63). The basis of their technique is to factor $\tilde{Z}^M$ using the singular-value decomposition (SVD). Using an SVD, one can compress the matrix by only retaining the larger singular values. This also allows fast computation of matrix–vector products. This, of course, requires an efficient procedure to compute the SVD. For matrices generated from integral equations, [23] develops an efficient recursive process to compute the SVD. In [3], an approximate technique is presented to compute (63) indirectly by ignoring detail in long-range interactions. This is, in fact, the crux of all the above-mentioned techniques.

D. Efficient Calculation of Eddy-Current Losses

As it stands, the derivations of Section II are not directly applicable to the above analysis unless an unrealistic 2-D approximation is used. A three-dimensional approach, on the other hand, requires numerical integration calculations that are at least four orders of magnitude more expensive to perform. To see this, note that instead of a one-dimensional integral for the magnetic vector potential, we would require a 2-D integral. Also, integration of A over the source and field cross sections will add two to four more dimensions. Finally, integration of A along the path of the field will involve one final line integral, adding at least one dimension to the problem. The 2-D approximation, though, only involves an integral of one dimension. This is because the integrations over the cross sections can be performed analytically and the integration along the path of the field is trivial to

compute due to the z-direction invariance inherent in the 2-D approach.

On the other hand, the free-space calculation of the magnetic vector potential is exact and the mutual inductance between filaments may be performed in closed form. To include the cross section of the conductors requires numerical integration over the volume of the conductors. The geometric mean distance (GMD) approximation [24], [25], on the other hand, yields closed-form results for the case of parallel rectangular cross sections. Thus, each matrix element computation can be performed in closed form. It has been found experimentally that the GMD approximation computes the free-space inductance value to a high precision for conductors over insulating or semi-insulating substrates. [26]–[29], [3].[2]

In order to retain the accuracy of the free-space GMD approximation and the simplicity of the 2-D approximation, we propose a hybrid calculation. As already noted, due to linearity of the partial differential (9), we can write the general solution as follows:

$$A(x, y, z) = A_{\text{free space}} + A_{\text{substrate}}. \tag{64}$$

The first term is the magnetic vector potential computed in free space. The second term is the magnetic vector potential resulting from the substrate currents. Note that the substrate currents are response currents, whereas the free-space currents are impressed currents. The response currents are not known *a priori*, thus, the second term cannot be computed directly. However, we have already factored $A(x, y)$ in this form in (37). Thus, we may compute the first term directly, using the GMD approximation to simplify the calculations. The second term is computed using the 2-D approximation developed in Section II. Since the substrate effects are secondary in nature at frequencies of interest, the error in the above approximation tends to be second order, yielding accurate overall results.

Hence, computation of (63) proceeds to the following two stages:

$$\tilde{Z}^{M}_{i,j} = \tilde{Z}^{M,F}_{i,j} + \tilde{Z}^{M,S}_{i,j} \tag{65}$$

where the second term is computed from

$$\tilde{Z}^{M,S}_{i,j} = \frac{-\mu j\omega}{2\pi} \int_0^\infty g(m)\, dm \tag{66}$$

$$g(m) = \cos\big(m(x - x_0)\big) \frac{e^{-m|y-y_0|}}{m} \Gamma(m) K(m, w). \tag{67}$$

The real part of the above matrix element represents the eddy-current losses, and the imaginary part represents the decrease in inductance due to image currents flowing in the substrate. Note that the kernel K is computed by integrating over the cross section of the source and field points. This term is unity for filaments, and for thin conductors of width w, it is given by the bracketed expression of (58).

Note that the purpose of calculating $\tilde{Z}^{M}$ is to obtain and account for the nonuniform current distribution in the volume of the conductors. This nonuniformity arises primarily from the nonuniform mutual inductive effects that are contained in the first term of (65). Since the losses computed from (66) tend to be uniform and do not influence the skin and proximity effects, one can reduce the number of calculations of (66) by including the substrate reflection terms at the conductor stage rather than at the sub-conductor stage. Thus, we may include the computation of (66) by simply adding it to the reduced matrix term directly. This reduces the number of computations from $O(N^2 \cdot M^2)$ to $O(N^2)$, where there are N conductors divided into an average of M sub-conductors. The validity of this approach can be verified by calculating the equivalent resistance and inductance of a device both ways.

[2]It is interesting to note that the GMD approximation is, in essence, a 2-D approximation as the function $\log(r)$, the free-space 2-D Green function, is averaged over the cross section of the conductors.

E. Eddy-Current Loss for Square Spiral Inductor

To compute (66) for the case of a spiral inductor, one can take advantage of the 2-D symmetries of Fig. 3 to further reduce the number of calculations from $O(N^2)$ to $O(2N)$. The complete substrate reflection matrix may be computed using the following algorithm.

Let $Z^{M,S} : 2N \times 2N$ be the substrate partial inductance matrix. Let

$$f_{r,i}(|d_{src} - d_{fld}|, h_{src} + h_{fld}, w) = \int_0^\infty dm \frac{e^{-m(h_{src}+h_{fld})}}{m} \Gamma_{r,i}(m) K(m, w) \cdot \cos\big(m(d_{src} - d_{fld})\big).$$

Also let $r_{src}(d_{src}, h_{src})$ represent the (x, y) coordinates of the source and $r_{fld}(d_{fld}, h_{fld})$ represent the field coordinates. Finally, the geometric mean length of two segments is given by

$$L^{GML}_{i,j} = \sqrt{L_i L_j}$$

```
begin:
Diagonal terms: Z^GML_{i,j} = L^GML_{i,j} f(0, 2b, w)
for j = 2 : N
  Z^{M,S}_{1,j} = L^GML_{1,j} f((j-1)s, 2b, w)
end
for i = 2 : N
  for j = i+1 : N
    Z^{M,S}_{i,j} = (L^GML_{i,j} / L^GML_{i-1,j-1}) Z^{M,S}_{i-1,j-1}
  end
end
for j = N+2 : 2N
  Z^{M,S}_{1,j} = L^GML_{1,j} f(L_i + (j-(N+2))s, 2b, w)
end
for i = 2 : N
  for j = N+2 : 2N
    Z^{M,S}_{i,j} = (L^GML_{i,j} / L^GML_{i-1,j-1}) Z^{M,S}_{i-1,j-1}
  end
end
for i = N+1 : 2N
  for j = N+2 : 2N
    Z^{M,S}_{i,j} = (L^GML_{i,j} / L^GML_{i-N,j-N}) Z^{M,S}_{i-N,j-N}
  end
end
let Z_{j,i} = Z_{i,j}
```

Note that the above algorithm involves only $O(2N)$ computations since the double loops only involve data transfer.

F. Complete PEEC Formulation

Consider the series interconnection of conductors, as shown in Fig. 5. Using the reduced partial inductance matrix discussed in the previous section, along with the reduced lossy capacitance matrix discussed in [7], one can form the following system of linear equations.

Let $i_{s,k} = (1/2)(i_k + i_{k+1})$ represent the average current flowing in the kth conductor. Similarly, let $v_{s,k} = (1/2)(v_k + v_{k+1})$ represent the average voltage of each conductor. Applying KCL and Kirchhoff's voltage law (KVL) at each node gives

$$i_k - i_{k+1} = \sum_{j=1}^{N} Y^C_{k,j} \left(\frac{v_j + v_{j+1}}{2} \right) \tag{68}$$

$$v_k - v_{k+1} = \sum_{j=1}^{N} Z^M_{k,j} \left(\frac{i_j + i_{j+1}}{2} \right) \tag{69}$$

where Y^C represents the complex lossy capacitive admittance matrix, which is computed directly in [7]. Z^M is computed using (65). Note that these matrices are compressed or reduced in order and contain the effects of nonuniform charge and current distribution in each conductor. All loss mechanisms relevant at microwave frequencies are thus contained in these matrices. Y^C is frequency dependent and includes electrically induced substrate losses. Z^M includes ohmic losses, skin and proximity effects, and magnetically induced substrate losses.

Writing (68) and (69) in the standard modified nodal analysis (MNA) matrix notation, one obtains

$$\begin{pmatrix} -Y^C S & D \\ D & -Z^M S \\ J & 0 \end{pmatrix} \begin{pmatrix} v \\ i \end{pmatrix} = \begin{pmatrix} 0 \\ v_{s1} \\ v_{s2} \end{pmatrix}. \tag{70}$$

The last two rows of the above matrix simply enforce boundary conditions at the input and output terminals, which forces these terminals to equal the impressed voltage. Note the right-hand side of the above matrix contains $2N$ zero terms followed by the impressed voltages. The matrix S simply averages, whereas the matrix D subtracts adjacent node voltages and terminal currents. In the continuous limit, these matrix operators represent integration and differentiation, respectively.

The above system can be solved numerically using Gaussian elimination. Since a typical device involves hundreds or at most thousands of elements, numerical packages such as LAPACK [30] can be used to efficiently compute the inverse of (70). LAPACK uses BLAS level–3 routines which utilize the system cache to maximize memory throughput. For larger systems, iterative solutions are more appropriate.

Similarly, (66) can be computed numerically using QUADPACK [31]. This package contains code to efficiently calculate (66) and the results converge much faster than using Romberg integration, as is done in [32]. The above algorithms have been assembled into the user-friendly package *Analysis and Simulation of Inductors and Transformers for ICs* (*ASITIC*).[3] This tool can be used to analyze spiral inductors, transformers, metal interconnect, and other similar structures residing over a multilayer Si substrate.

V. Examples and Measurement Results

A. Single-Layer Substrate

The magnetostatic problem of a one-layer conductive substrate has been the subject of detailed investigations. References [12]–[14] derive and compute the integrals of Section II. In particular, [13] discusses numerical and analytical techniques to compute the integral. In our research, we found numerical integration sufficient and, thus, analytical integration was not our main focus. The solution of the one-layer problem is summarized by the following reflection coefficient:

$$\Gamma(m) = \frac{\gamma - m}{\gamma + m} e^{-2my_0} \tag{71}$$

where y_0 is the source y-coordinate. For the case of a one-layer substrate, we found the following analytical representation:

$$Z_{ij} = -200\pi j\omega \left(g(z_1) + g(z_2) + \frac{1}{z_1^2} + \frac{1}{z_2^2} \right) \tag{72}$$

where

$$z_{1,2} = (2b \pm (d_i - d_j)j)(j-1)\frac{\sqrt{800\pi\sigma\omega}}{2} \tag{73}$$

and

$$g(z) = \int_0^\infty e^{-cz}\sqrt{c^2 - 1}\, dc. \tag{74}$$

The above integral can be represented as follows:

$$g(z) = \frac{K_1(z)}{z} + \pi j \frac{I_1(z)}{2z} - \frac{jz}{3} {}_pF_q \left(1, \left\{ \frac{3}{2}, \frac{5}{2} \right\}; \frac{z^2}{4} \right) \tag{75}$$

where I_1 and K_1 are first-order modified Bessel functions of the first- and second-kind, respectively, and ${}_pF_q$ is a generalized hypergeometric function [33]. Since (74) represents the contour integration of an analytic function, its value is path independent. Using this property, integral representations of the various standard mathematical functions can be used to derive the above result.

However, as previously noted, numerical integration is often faster than the direction computation of (75), and this approach will be pursued for the more complicated geometries where analytical results are more difficult to obtain.

B. Two-Layer Substrate

For the two-layer problem, the equations of Section II are set up and involve six equations in six unknowns. The solution can be simplified into the following form:

$$\Gamma(m) = e^{-2my_0} \frac{\gamma_2(m - \gamma_3) - (\gamma_2^2 - m\gamma_3)\tanh(t\gamma_2)}{\gamma_2(m + \gamma_3) + (\gamma_2^2 + m\gamma_3)\tanh(t\gamma_2)} \tag{76}$$

[3][Online]. Available: http://www.eecs.berkeley.edu/niknejad

TABLE I
SPIRAL $L27$ PHYSICAL DIMENSIONS

Spiral Name	1.27
Outer Length (μm)	250
Metal Width W (μm)	10.5
Metal Spacing S (μm)	3
No. of Turns N	7.75
Metal Layer	M5
Metal Sheet Resis. (mΩ/sq)	35
Metal Thickness (μm)	0.91
Capacitance of Substrate (aF/μm ^{2})	6.12

where y_0 denotes the source y-coordinate and t is the thickness of the top substrate layer. Note that (76) reduces to (71) as $t \to \infty$. It can also be shown that

$$\lim_{m \to 0} \frac{\Im(\Gamma(m))}{m} < \infty. \tag{77}$$

Also, since (76) is exponentially decreasing for large m, numerical integration of (66) converges rapidly.

The above result along with (66) can be used to solve for the eddy-current losses and decrease in inductance due to the conductive substrate.

C. Measurement Results

Several planar and nonplanar spiral inductors have been fabricated in National Semiconductor's 0.25-μm CMOS-8 process. This process utilizes a bulk substrate of 10 $\Omega \cdot$cm, sufficiently resistive so that eddy currents play a minor part in the bulk. However, the top layer of Si is fairly conductive at 15×10^{-4} $\Omega \cdot$cm. The thickness of this layer is less than 1 μm, but this is enough to cause significant eddy-current loss.

The layout of a spiral inductor is summarized in Table I. As shown in Fig. 4, spiral inductor $L27$ is a planar device utilizing the top metal layer.

Measurements are performed using a ground–signal–ground (G–S–G) coplanar waveguide pad configuration. The s-parameters are measured using an HP 8719C Network Analyzer. G–S–G coplanar cascade probes are used and the setup is calibrated using a Cascade Microtech 832 210 calibration substrate. The open-pad y-parameters are also measured and subtracted from the measured y-parameters to remove the pad capacitance and loss.

Measured s-parameters for inductor $L27$ are shown in Fig. 6. The simulated and measured results match well. The discrepancy above the self-resonant frequency is in the capacitive region where we are less interested in the device. Notice that the inductor self-resonates at a frequency of 4.25 GHz. Simulations using ASITIC predicted a self-resonant frequency of 4.15 GHz. The simulations are performed on a Pentium II 400-MHz machine running the Linux operating system. Each frequency point requires less than 10 s of computation. In Fig. 7, we plot the effective value of inductance. This is derived using a one-to-one transformation of the s-parameters into π-parameters [3]. Again, a good match is observed between the theory and measurements. The inductance decrease is due mostly to the capacitive effects rather than the inductive effects. Inductance value decreases slightly due to skin effect and eddy currents in the substrate, but the main reason for the decrease is that energy is coupled from port to port through the winding capacitance at higher frequencies.

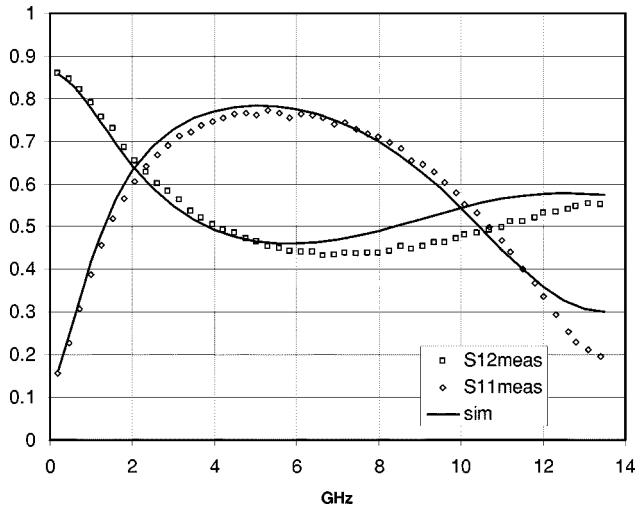

(a)

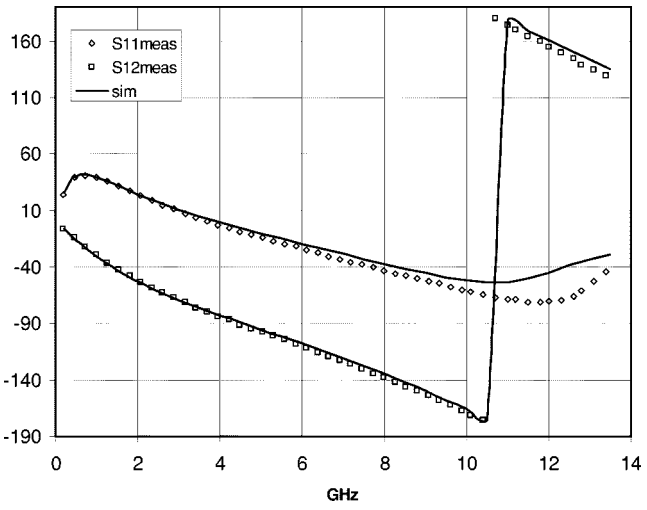

(b)

Fig. 6. Measured and simulated s-parameters (magnitude and phase) of spiral inductor $L27$.

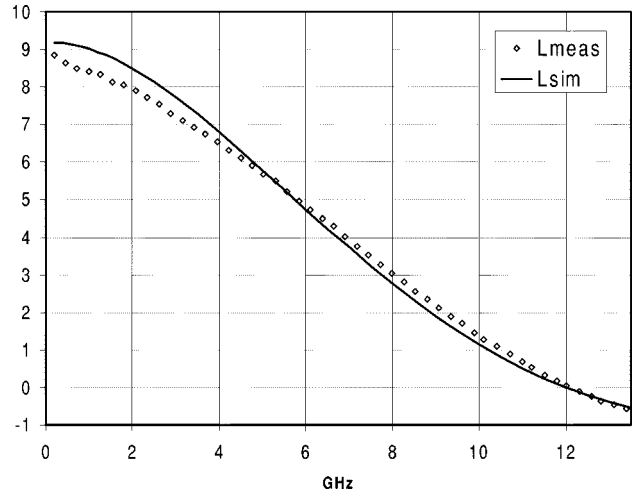

Fig. 7. Measured and simulated inductance (imaginary component of Y_{21}) of spiral inductor $L27$.

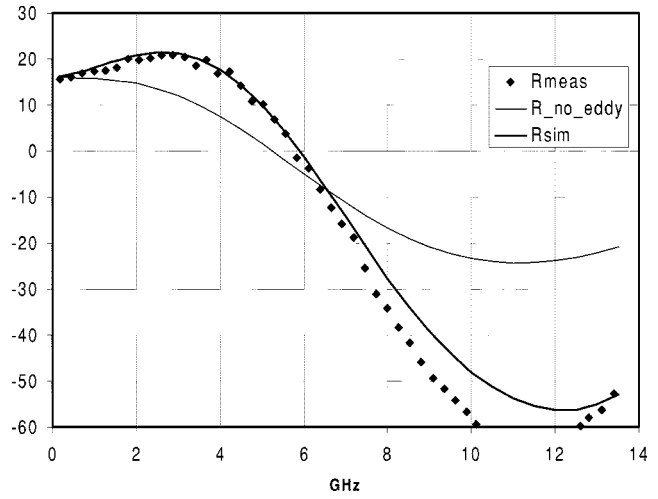

Fig. 8. Measured and simulated resistance (real component of Y_{21}) of spiral inductor $L27$.

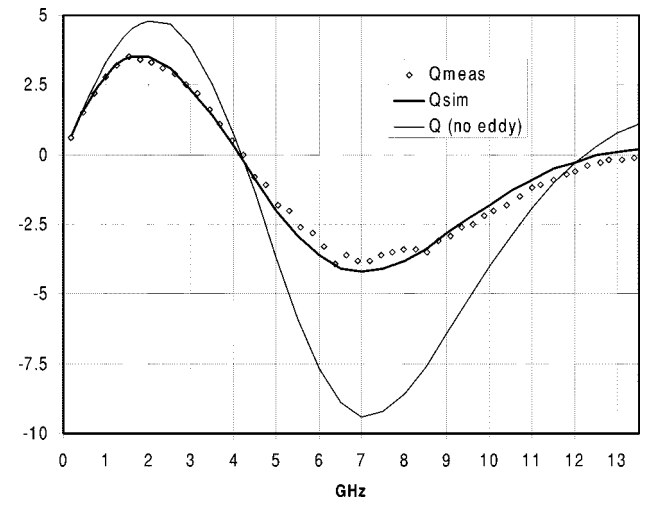

Fig. 9. Measured and simulated Q factor (imaginary over real component of Y_{21}) of spiral inductor $L27$.

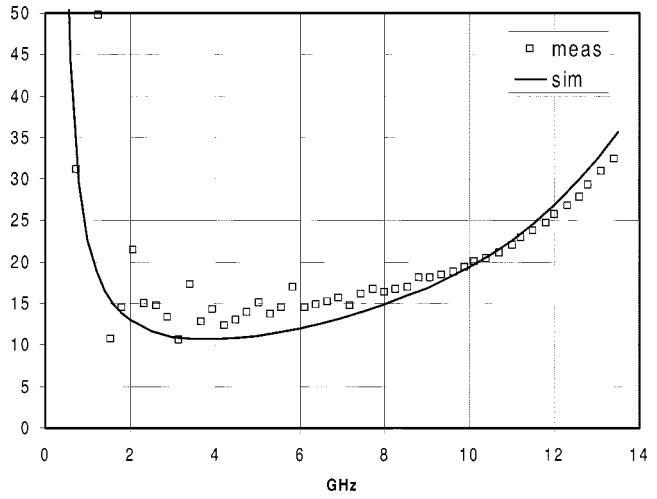

Fig. 10. Measured and simulated substrate resistance of spiral inductor $L27$.

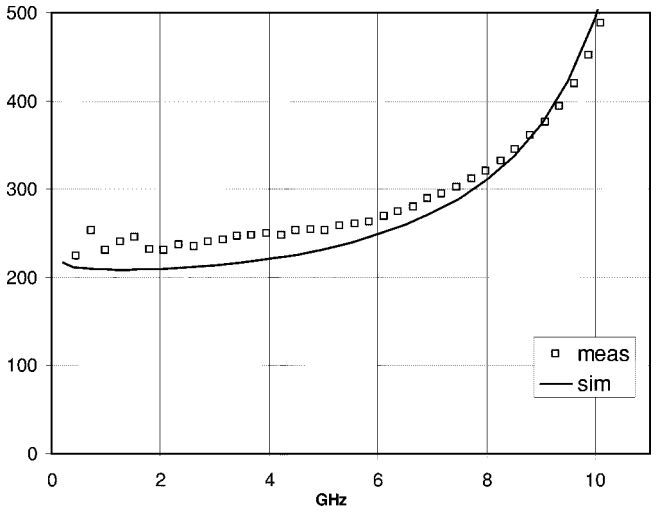

Fig. 11. Measured and simulated substrate capacitance of spiral inductor $L27$.

Fig. 8 shows the effective value of series resistance as a function of frequency. Two simulations are performed: with and without eddy-current losses. As evident in this figure, eddy-current losses are critical to model. The variation in frequency of the series resistance is due to various competing effects. Skin effect and proximity effects increase the series resistance, but beyond 1 GHz, this is swamped by the increase from eddy currents. At higher frequencies, more energy is transported capacitively and, consequently, the resistance decreases and eventually becomes negative. The real part of the total input impedance looking into each port, of course, is positive at all frequencies.

The Q factor, the ratio between the imaginary and real part of the input impedance, is plotted in Fig. 9. Again, a good match is observed between the theory and measurements. Note that negative Q factor implies that the device is acting as a capacitor rather than an inductor. In reality, this plot is misleading, as it implies a Q of zero at self-resonance. A better way to calculate Q is given in [3], but for comparison, the given definition is better since it involves a minimal transformation of the measured s-parameters. The substrate resistance and capacitance are also shown in Figs. 10 and 11. The overall shape of both curves matches the measurements well. The low-frequency substrate resistance measurements are noisy due to measurement error.

VI. Conclusion

In this paper, we have presented 2-D eddy-current loss equations applicable to transmission lines and interconnect over a conductive substrate. The results are also applicable to spiral inductors and transformers fabricated over conductive substrates. We have proposed a hybrid calculation of the magnetic vector potential to retain the accuracy of a three-dimensional free-space formulation while exploiting the simplicity of the 2-D eddy-current loss formulation. Measurement results confirm the validity of our approach.

Acknowledgment

The authors wish to greatly acknowledge National Semiconductor, Sunnyvale, CA, for the fabrication of the test structures. The authors also greatly appreciate A. Eldredge, Silicon Laboratories, Austin, TX, for help in the layout and verification of the test structures.

REFERENCES

[1] J. Craninckx and M. S. J. Steyaert, "A 1.8-GHz low-phase-noise CMOS VCO using optimized hollow spiral inductors," *IEEE J. Solid-State Circuits*, vol. 32, pp. 736–744, May 1997.

[2] T. Huan-Shang, L. Jenshan Lin, R. C. Frye, K. L. Tai, M. Y. Lau, D. Kossives, F. Hrycenko, and C. Young-Kai, "Investigation of current crowding effect on spiral inductors," in *IEEE MTT-S Technol. Wireless Applicat. Symp. Dig.*, 1997, pp. 139–142.

[3] A. M. Niknejad and R. G. Meyer, "Analysis, design, and optimization of spiral inductors and transformers for Si RF ICs," *IEEE J. Solid-State Circuits*, vol. 33, pp. 1470–1481, Oct. 1998.

[4] A. E. Ruehli, "Inductance calculations in a complex integrated circuit environment," *IBM J. Res. Develop.*, vol. 16, pp. 470–481, Sept. 1972.

[5] W. T. Weeks, L. L. Wu, M. F. McAllister, and A. Singh, "Resistive and inductive skin effect in rectangular conductors," *IBM J. Res. Develop.*, vol. 23, pp. 652–660, Nov. 1979.

[6] A. E. Ruehli and H. Heeb, "Circuit models for three-dimensional geometries including dielectrics," *IEEE Trans. Microwave Theory Tech*, vol. 40, pp. 1507–1516, July 1992.

[7] A. M. Niknejad, R. Gharpurey, and R. G. Meyer, "Numerically stable green function for modeling and analysis of substrate coupling in integrated circuits," *IEEE Trans. Computer-Aided Design*, vol. 17, pp. 305–315, Apr. 1998.

[8] R. Gharpurey and R. G. Meyer, "Analysis and simulation of substrate coupling in integrated circuits," *Int. J. Circuit Theory Applicat.*, vol. 23, pp. 381–394, July-Aug. 1995.

[9] "1997 IEEE Custom Integrated Circuits Conf. Author Interview," unpublished.

[10] S. Ramo, J. R. Whinnery, and T. Van Duzer, *Fields and Waves in Communication Electronics*, 3rd ed. New York: Wiley, 1994, pp. 324–330.

[11] D. W. Trim, *Applied Partial Differential Equations*. Boston, MA: PWS-KENT, 1990.

[12] R. L. Stoll, *The Analysis of Eddy Currents*. Oxford, U.K.: Clarendon, 1974.

[13] H. Poritsky and R. P. Jerrard, "Eddy-current losses in a semi-infinite solid due to a nearby alternating current," *Trans. Amer. Inst. Elect. Eng.*, pt. 1, vol. 73, pp. 97–106, May 1954.

[14] J. A. Tegopoulos and E. E. Kriezis, *Eddy Currents in Linear Conducting Media*. Amsterdam, The Netherlands: Elsevier, 1985.

[15] W. G. Hurley and M. C. Duffy, "Calculation of self and mutual impedances in planar magnetic structures," *IEEE Trans. Magn.*, vol. 31, pp. 2416–22, July 1995.

[16] W. G. Hurley and M. C. Duffy, "Calculation of self- and mutual impedances in planar sandwich inductors," *IEEE Trans. Magn.*, vol. 33, pp. 2282–2290, May 1997.

[17] J. R. Wait, *Geo-Electromagnetism*. New York: Academic, 1982.

[18] S. F. Mahmoud and E. Beyne, "Inductance and quality-factor evaluation of planar lumped inductors in a multilayer configuration," *IEEE Trans. Microwave Theory Tech.*, vol. 45, pp. 918–923, June 1997.

[19] J. Lee, A. Karl, A. A. Abidi, and N. G. Alexopoulos, "Design of spiral inductors on silicon substrates with a fast simulator," in *European Solid-State Circuits Conf.*, Sept. 1998.

[20] G. F. Roach, *Green's Functions*, 2nd ed. Cambridge, U.K.: Cambridge Univ. Press, 1982.

[21] M. Kamon, M. J. Ttsuk, and J. K. White, "FASTHENRY: A multipole-accelerated 3-D inductance extraction program," *IEEE Trans. Microwave Theory Tech.*, vol. 42, pp. 1750–1758, Sept. 1994.

[22] L. Greengard and V. Rokhlin, "A fast algorithm for particle simulations," *J. Comput. Phys.*, vol. 135, pp. 280–292, Aug. 1997.

[23] S. Kapur and D. E. Long, "IES3: A fast integral equation solver for efficient 3-dimensional extraction," in *1997 IEEE/ACM Int. Computer-Aided Design Conf.*, 1997, pp. 448–455.

[24] H. M. Greenhouse, "Design of planar rectangular microelectronic inductors," *IEEE Trans. Parts, Hybrids, Packag.*, vol. PHP-10, pp. 101–109, June 1974.

[25] F. W. Grover, *Inductance Calculations*. New York: Van Nostrand, 1946.

[26] D. M. Krafcsik and D. E. Dawson, "A closed-form expression for representing the distributed nature of the spiral inductor," in *IEEE Microwave Millimeter-Wave Monolithic Circuits Symp. Dig.*, 1986, pp. 87–92.

[27] E. Pettenpaul and H. Kapusta *et al.*, "CAD models of lumped elements on GaAs up to 18 GHz," *IEEE Trans. Microwave Theory Tech.*, vol. 36, pp. 294–304, Feb. 1988.

[28] N. M. Nguyen and R. G. Meyer, "Si IC-compatible inductors and *LC* passive filters," *IEEE J. Solid-State Circuits*, vol. 27, pp. 1028–1031, Aug. 1990.

[29] J. R. Long and M. A. Copeland, "The modeling, characterization, and design of monolithic inductors for silicon RF IC's," *IEEE J. Solid-State Circuits*, vol. 32, pp. 357–369, Mar. 1997.

[30] J. Dongarra and J. Demmel, "LAPACK: a portable high-performance numerical library for linear algebra," *Supercomput.*, vol. 8, pp. 33–38, Nov. 1991.

[31] R. Piessens *et al.*, *Quadpack: A Subroutine Package for Automatic Integration*. Berlin, Germany: Springer-Verlag, 1983.

[32] S. Wolfram, *The Mathematica Book*, 4th ed. Cambridge, U.K.: Cambridge Univ. Press, 1999.

[33] M. Abramowitz and I. A. Stegun, *Handbook of Mathematical Functions with Formulas, Graphs, and Mathematical Tables*. New York: Wiley, 1972.

Ali M. Niknejad (S'92–M'00) was born in Tehran, Iran, on July 29, 1972. He received the B.S.E.E. degree from the University of California at Los Angeles, in 1994, and the M.S. and Ph.D. degrees in electrical engineering from the University of California at Berkeley, in 1997 and 2000, respectively.

He joined Silicon Laboratories, Austin TX, as a Design Engineer, where he is currently engaged in the design and research of CMOS RF integrated circuits (RFICs). His current research interests include RF/microwave integrated circuit (IC) design, modeling of passive devices, package and substrate coupling analysis, digital wireless communication systems, numerical methods in electromagnetics, and RF computer-aided design (CAD).

Robert G. Meyer (S'64–M'68–SM'74–F'81) was born in Melbourne, Australia, on July 21, 1942. He received the B.E., M.Eng.Sci., and Ph.D. degrees in electrical engineering from the University of Melbourne, Melbourne, Australia, in 1963, 1965, and 1968, respectively.

In 1968, he was an Assistant Lecturer in the Electrical Engineering Department, University of Melbourne. Since September 1968, he has been with the Department of Electrical Engineering and Computer Sciences, University of California at Berkeley, where he is currently a Professor. His current research interests are high-frequency analog integrated-circuit design and device fabrication. He has acted as a consultant on electronic circuit design for numerous companies in the electronics industry. He has co-authored *Analysis and Design of Analog Integrated Circuit* (New York: Wiley, 1993), edited *Integrated Circuit Operational Amplifiers* (New York: IEEE Press, 1978), and co-edited *Integrated Circuits for Wireless Communications*, (Piscataway, NJ: IEEE Press, 1999).

Dr. Meyer was President of the IEEE Solid-State Circuits Council and was an associate editor of the IEEE JOURNAL OF SOLID-STATE CIRCUITS and the IEEE TRANSACTIONS ON CIRCUITS AND SYSTEMS.